INFLUENCE OF THE THIRD INVARIANT, BY THE LODE ANGLE, ON THE MECHANICAL BEHAVIOR OF DUCTILE MATERIALS

João V. Sahadi, joao_sahadi@aluno.unb.br
Lucival Malcher, malcher@unb.br
Raniere S. Neves, raniere_neves@aluno.unb.br
Natália S. I. Aoyama, natalia_seyko@aluno.unb.br
UnB – University of Brasília, Faculty UnB Gama, Distrito Federal - Brazil

Thiago Doca, thiago.doca@fe.up.pt
Filipe X. C. Andrade, filipe.xavier@fe.up.pt
Fábio J. P. Reis, fabio.reis@fe.up.pt
IDMEC – Institute of Mechanical Engineering, Faculty of Engineering, University of Porto, Porto, Portugal.

Abstract. *In this paper, it is suggested a numerical study, based on an implicit integration algorithm, for a new elasto-plastic constitutive model proposed by Bai & Wierzbicki, where the influence of the third invariant of the deviatoric stress tensor, by the so-called Lode angle, is contemplated in the behavior of the ductile materials. In the first part, the constitutive equations related with Bai & Wierzbicki elasto-plastic model is presented as well as an implicit numerical integration algorithm, proposed by Malcher and co-authors, which is based on the operator split methodology. Besides that, the algorithm is implemented in an "in house" academic finite element environment. Then, some conventional specimens are selected, as a cylindrical smooth bar, a cylindrical notched bar and a flat grooved plate specimen, in order to carried out numerical test to verify the influence of the third invariant of the deviatoric stress tensor in the behavior of material and in the prediction of the correct location to crack initiation, by the equivalent plastic strain as the fracture indicator role. The aluminum alloy 2024-T351, which is strongly dependent on both pressure and Lode angle, was chosen and the material properties are used to set up the constitutive formulation. The influence of the third invariant is evaluated by numerical and experimental results for the reaction versus displacement curve, and the ability to predict the crack initiation is studied by the evolution of the equivalent plastic strain at the critical point and the contour of this internal variable around the finite element mesh.*

Keywords*: elasto-plastic model, operator split method, influence of the third invariant.*

1. INTRODUCTION

One of the most commonly used models to describe the behavior of metals is the von Mises model, which is based on the J_2 theory. The von Mises model can be regarded as "pressure-insensitive" since it assumes that the effects of hydrostatic stress are negligible on the plastic flow rule. In general, the hydrostatic stress is responsible for controlling the size of the yield surface (Bai, 2008). Furthermore, the von Mises model is independent of the third invariant of the deviator stress tensor, which is denoted here by J_3. The third invariant is a parameter used in the definition of the Lode angle or Azimuth angle, which is responsible for the shape of the yield surface (Bardet, 1999; Bai, 2008).

The importance of the hydrostatic stress and Lode angle has been recognized by several authors and introduced into the constitutive description of some materials such as soil and rock. In the case of ductile materials, many researchers have done extensive experimental studies as Richmond & Spitzing (1980 and 1984), who were the first researchers to study the effects of the pressure on yielding of aluminum alloys, Bardet (1990), who proposed a study to describes the Lode angle dependence for some constitutive model, Wilson (2002), which conducted studies to notched 2024-T351 aluminum bars in tensile test and verified the importance of these effects, Brunig *et al* (1999;2000) and Bai *et al* (2007) proposed a constitutive model with three invariants to be applied in metal plasticity and fracture.

Ductile fracture is a local phenomenon and the state of stress and strain in the expected fracture locus must be determined with accuracy. The fracture initiation is often preceded by large plastic deformation and there are considerable stress and strain gradients around the point of fracture. In this case, the J_2 theory is not accurate enough and more refined plasticity models have to be introduced. Based on what was explained, the Bai & Wierzbicki elasto plastic model (Bai, 2008), which is pressure sensitive and Lode angle dependent, will be widely studied in this work, regarding the contribution of both pressure and Lode angle parameters in the plastic flow rule for ductile materials.

2. CONSTITUTIVE FORMULATION AND NUMERICAL INTEGRATION

2.1. Constitutive formulation

Bai & Wierzbicki (2007) have proposed an elasto-plastic model that includes the effect of pressure through the triaxiality ratio and the effect of the third invariant through the Lode angle. The effects are introduced by redefining the

hardening rule of the material. In the classic von Mises model, the hardening rule is only a function of the accumulated plastic strain $\sigma_y(\bar{\varepsilon}^p)$ and, in the Bai & Wierzbicki model, the hardening rule is a function of the accumulated plastic strain, the triaxiality ratio and the parameter $\mu(\theta)$, which is a function of the Lode angle, $\sigma_y(\bar{\varepsilon}^p, \eta, \mu)$. Thus, the new definition of the hardening rule can be obtained according Equation 1:

$$\sigma_y(\bar{\varepsilon}^p, \eta, \mu) = \sigma_y(\bar{\varepsilon}^p).\left[1 - C_\eta(\eta - \eta_0)\right].\left[C_\theta^s + (C_\theta^{ax} - C_\theta^s)\left(\mu - \frac{\mu^{m+1}}{m+1}\right)\right] \tag{1}$$

where, $\sigma_y(\bar{\varepsilon}^p)$ is the material strain hardening function, $C_\eta, C_\theta^s, C_\theta^{ax}$, and m are experimental parameters, η represents the triaxiality ratio, which is defined as a ratio between the pressure and the von Mises equivalent stress, $\eta = p/q$, η_0 is the reference value to triaxiality ratio, μ is a parameter defined as a function of the Lode angle through the equation below:

$$\mu = \frac{cos(\pi/6)}{1 - cos(\pi/6)}\left[\frac{1}{cos(\theta - \pi/6)} - 1\right] = 6.4641[sec(\theta - \pi/6) - 1] \tag{2}$$

where $\boldsymbol{\theta}$ represents the Lode angle, which can be determined according to Equation 3:

$$\theta = \tan^{-1}\left\{\frac{1}{\sqrt{3}}\left[2.\left(\frac{S_2 - S_3}{S_1 - S_3}\right) - 1\right]\right\} \tag{3}$$

According to Bai (2008), the effect of the triaxiality ratio and Load angle are included on the hardening rule through the parameters $\left[\mathbf{1} - \boldsymbol{C_\eta}(\boldsymbol{\eta} - \boldsymbol{\eta_0})\right]$ and $\left[\boldsymbol{C_\theta^s} + (\boldsymbol{C_\theta^{ax}} - \boldsymbol{C_\theta^s})\left(\boldsymbol{\mu} - \frac{\boldsymbol{\mu^{m+1}}}{\boldsymbol{m+1}}\right)\right]$, respectively. The new yield criterion replaces the standard hardening rule from $\boldsymbol{\sigma_y}(\bar{\boldsymbol{\varepsilon}}^{\boldsymbol{p}})$ to $\boldsymbol{\sigma_y}(\bar{\boldsymbol{\varepsilon}}^{\boldsymbol{p}}, \boldsymbol{\eta}, \boldsymbol{\mu})$ on the $\boldsymbol{J_2}$ theory, such that the yield criterion can be re-written as:

$$\Phi = q - \sigma_y(\bar{\varepsilon}^p, \eta, \mu) = q - \sigma_y(\bar{\varepsilon}^p).\left[1 - C_\eta(\eta - \eta_0)\right].\left[C_\theta^s + (C_\theta^{ax} - C_\theta^s)\left(\mu - \frac{\mu^{m+1}}{m+1}\right)\right] \tag{4}$$

Through Equation 4, we can define the parameters $A(\eta)$ and $B(\mu)$ according the Equations 5 and 6, respectively, as:

$$A(\eta) = \left[1 - C_\eta(\eta - \eta_0)\right] \tag{5}$$

$$B(\mu) = \left[C_\theta^s + (C_\theta^{ax} - C_\theta^s)\left(\mu - \frac{\mu^{m+1}}{m+1}\right)\right] \tag{6}$$

Thus, the Equation 4 can be re-written as:

$$\Phi = q - \sigma_y(\bar{\varepsilon}^p).A(\eta).B(\mu) \tag{7}$$

The influence of the experimental parameters $\left(C_\eta, C_\theta^s, C_\theta^{ax}, \eta_0, m\right)$ on the behavior of the constitutive model can be analyzed as follows. The parameter C_η is a material constant and needs to be experimentally calibrated. This parameter describes the hydrostatic stress effect on material plasticity. If $C_\eta = 0$, the model loses the dependence of the triaxiality ratio or the hydrostatic stress effect and recovers, as a limiting case, the behavior of the von Mises model.

The triaxiality reference, η_0, depends on the type of test applied and the geometry of the specimen. For the smooth bar under tensile test, the parameter takes value equal $1/3$. However, for cylindrical specimen, in compressive test, $\eta_0 = -1/3$, for torsion and shear test $\eta_0 = 0$. The hydrostatic stress effect introduced by Bai & Wierzbicki is a linear function and for some researcher (Karr *et al*, 1989), claim that those effect is non-linear for some materials, such as ice. Analyzing the third invariant effect, the experimental parameter C_θ^{ax} can assume one of two forms, according the type of loading (tension/compression) applied:

$$C_\theta^{ax} = \begin{cases} C_\theta^t & for \quad \bar{\theta} \geq 0 \\ C_\theta^c & for \quad \bar{\theta} < 0 \end{cases} \tag{8}$$

The parameter C_θ^s also depends on the type of test. For example, if a smooth bar is used in a tensile test $C_\theta^t = 0$, if a torsion test $C_\theta^s = 1$, if a cylindrical specimen is used in a compressive test $C_\theta^c = 1$. The convexity of the yield surface is

controlled by the rations of these parameters. The range of the parameter μ is between $0 \leq \mu \leq 1$. When $\mu = 0$ it corresponds to plane strain or shear condition, when $\mu = 1$ it corresponds to axisymmetric problem. The introduction of the term $\mu^{m+1}/m+1$ is done to assume the smoothness of yield surface and is differentiability with respect to Lode angle around $\mu = 1$. More details about the calibration of the material parameters can be verified in Bai *et al* (2007). In the *Box 1*, the summary of the Bai & Wierzbicki´s model is presented.

Box 1. Bai & Wierzbicki's model with isotropic hardening.

(i) Elasto-plastic split of strain tensor

$$\boldsymbol{\varepsilon} = \boldsymbol{\varepsilon}^e + \boldsymbol{\varepsilon}^p$$

(ii) Elastic law

$$\boldsymbol{\sigma} = \mathbf{D}^e : \boldsymbol{\varepsilon}^e$$

(iii) Yield function

$$\Phi = q - \sigma_y(\bar{\varepsilon}^p).A.B$$

with A and B given by:

$$A = \left[1 - C_\eta(\eta - \eta_0)\right] \quad ; \qquad B = \left[C_\theta^s + (C_\theta^{ax} - C_\theta^s)\left(\mu - \frac{\mu^{m+1}}{m+1}\right)\right]$$

and, $\mu = \frac{cos(\pi/6)}{1-cos(\pi/6)}\left[\frac{1}{cos(\theta-\pi/6)} - 1\right]$

(iv) Plastic flow and evolution equation for $\dot{\bar{\varepsilon}}^p$

$$\dot{\boldsymbol{\varepsilon}}^p = \dot{\gamma}.\boldsymbol{N} = \dot{\gamma}.\left(\frac{3}{2q}.\alpha.\boldsymbol{S} + \frac{3}{2q}.\lambda.\boldsymbol{S^2} + \frac{1}{3}\beta.\boldsymbol{I}\right)$$

$$\dot{\bar{\varepsilon}}^p = \dot{\gamma}\sqrt{\alpha^2 + \lambda^2\frac{\boldsymbol{S^2}:\boldsymbol{S^2}}{\boldsymbol{S}:\boldsymbol{S}} + \frac{2.\beta^2}{9} + 2.\alpha.\lambda\frac{\boldsymbol{S}:\boldsymbol{S^2}}{\boldsymbol{S}:\boldsymbol{S}} + \frac{2.\lambda.\beta}{3.q}tr(\boldsymbol{S^2})}$$

and α, β and λ:

$$\alpha = 1 - \frac{\sigma_y(\bar{\varepsilon}^p)}{q}\left(C_\eta.B.\eta + A.D.\xi\right)$$

$$\beta = \frac{\sigma_y(\bar{\varepsilon}^p)}{q}\left[C_\eta.B - \frac{9.A.D}{2.q^2}\left(tr(\boldsymbol{\sigma^2}) - \frac{tr(\boldsymbol{\sigma})^2}{3}\right)\right]$$

$$\lambda = \frac{3.\sigma_y(\bar{\varepsilon}^p).A.D}{q^2}$$

$$D = (C_\theta^{ax} - C_\theta^s)(1-\mu^m)\frac{\cos(\pi/6)}{1-\cos(\pi/6)}\frac{\tan(\theta-\pi/6)}{\cos(\theta-\pi/6)}\frac{1}{\sin 3\theta}$$

(v) Loading/unloading criterion

$$\dot{\gamma} \geq 0\,, \qquad \Phi \leq 0\,, \qquad \dot{\gamma}\Phi = 0.$$

2.2. Numerical integration algorithm

In this part, a numerical integration algorithm for Bai & Wierzbicki model is taken, which was initially proposed by Malcher *et al* (2009). The algorithm was built, regarding an implicit solution and based on operator split methodology, which is especially suitable for the numerical integration of the evolution problem and have been widely used in computational plasticity (see Simo & Hughes, 1998; De Souza Neto *et al*., 2008). This method, which is used by Malcher *et al* (2009), consists of splitting the problem in two parts: an elastic predictor, where the problem is assumed to be elastic and, a plastic corrector, in which the system of residual equations comprising the elasticity law, plastic consistency and the rate equations is solved, taking the results of the elastic predictor stage as initial conditions. In the case of the yield condition has been violated, the plastic corrector stage is initiated and the Newton- Raphson procedure is used to solve the discretised equations. The Newton-Raphson procedure is chosen motivated by the quadratic rates of convergence achieved which results in return mapping procedures computationally efficient (see Simo & Hughes, 1998; De Souza Neto *et al*., 2008). The overall algorithm for numerical integration is summarized in Box 2.

Box 2. Fully implicit Elastic predictor/Return mapping algorithm for Bai & Wierzbicki model.

(i) Evaluate the elastic trial state: Given the incremental strain $\Delta\varepsilon$ and the state variables at t_n:

$$\boldsymbol{\varepsilon}_{n+1}^{e\,trial} = \boldsymbol{\varepsilon}_n^e + \Delta\boldsymbol{\varepsilon} \quad ; \quad \boldsymbol{S}_{n+1}^{trial} = 2G\boldsymbol{\varepsilon}_{n+1}^{e\,trial} \quad ; \quad p_{n+1}^{trial} = K\varepsilon_{v\,n+1}^{e\,trial}$$

$$q_{n+1}^{trial} = \sqrt{\frac{3}{2}}\left\|\boldsymbol{S}_{n+1}^{trial}\right\| \quad ; \quad \eta_{n+1}^{trial} = p_{n+1}^{trial}/q_{n+1}^{trial} \quad ; \quad r_{n+1}^{trial} = \left[\frac{27}{2}\det\left(\boldsymbol{S}_{n+1}^{trial}\right)\right]^{1/3}$$

$$\xi_{n+1}^{trial} = \left(r_{n+1}^{trial}/q_{n+1}^{trial}\right)^3 \quad ; \quad \theta_{n+1}^{trial} = \frac{1}{3}arccos\left(\xi_{n+1}^{trial}\right) \quad ; \quad \bar{\varepsilon}_{n+1}^{p\,trial} = \bar{\varepsilon}_n^p$$

$$\mu_{n+1}^{trial} = \frac{\cos(\pi/6)}{1-\cos(\pi/6)}.\left[sec\left(\theta_{n+1}^{trial} - {}^{\pi}/_{6}\right) - 1\right] \quad ; \quad A_{n+1}^{trial} = \left[1 - C_\eta\left(\eta_{n+1}^{trial} - \eta_0\right)\right]$$

$$B_{n+1}^{trial} = \left[C_\theta^s + (C_\theta^{ax} - C_\theta^s)\left(\mu_{n+1}^{trial} - \frac{{\mu_{n+1}^{trial}}^{m+1}}{m+1}\right)\right]$$

(ii) Check plastic admissibility:

IF $\Phi^{trial} = q_{n+1}^{trial} - \sigma_y\left(\bar{\varepsilon}_{n+1}^{p\,trial}\right).A_{n+1}^{trial}.B_{n+1}^{trial} \leq 0$ THEN
set $(\cdot)_{n+1} = (\cdot)_{n+1}^{trial}$ ***(elastic step)*** and go to *(v)*
ELSE go to (iii)

(iii) Return mapping ***(plastic step)***: *Solve the system of equations below for* $\Delta\gamma, p_{n+1}, f_{n+1}$ and R_{n+1}, *using Newton-Raphson method.*

$$\left\{\begin{array}{c} \mathbf{D}^{e-1}:\left(\boldsymbol{\sigma}_{n+1} - \boldsymbol{\sigma}_{n+1}^{trial}\right) + \Delta\gamma.\frac{3}{2q}.\alpha_{n+1}.\boldsymbol{S}_{n+1} + \frac{3}{2q}.\lambda_{n+1}.{\boldsymbol{S}_{n+1}}^2 + \frac{1}{3}\beta_{n+1}.\boldsymbol{I} \\ \bar{\varepsilon}_{n+1}^p - \bar{\varepsilon}_n^p - \Delta\bar{\varepsilon}^p = \bar{\varepsilon}_{n+1}^p - \bar{\varepsilon}_n^p - \Delta\gamma\sqrt{\zeta} \\ q_{n+1} - \sigma_y\left(\bar{\varepsilon}_{n+1}^p\right).A_{n+1}(\eta_{n+1}).B_{n+1}(\mu_{n+1}) \end{array}\right\} = \left\{\begin{array}{c}\mathbf{0}\\0\\0\end{array}\right\}$$

where,

$$\zeta = {\alpha_{n+1}}^2 + {\lambda_{n+1}}^2\frac{{\boldsymbol{S}_{n+1}}^2:{\boldsymbol{S}_{n+1}}^2}{\boldsymbol{S}_{n+1}:\boldsymbol{S}_{n+1}} + \frac{2.{\beta_{n+1}}^2}{9} + 2.\alpha_{n+1}.\lambda_{n+1}\frac{\boldsymbol{S}_{n+1}:{\boldsymbol{S}_{n+1}}^2}{\boldsymbol{S}_{n+1}:\boldsymbol{S}_{n+1}} + \frac{2.\lambda_{n+1}.\beta_{n+1}}{3.q_{n+1}}tr\left({\boldsymbol{S}_{n+1}}^2\right)$$

$$\alpha_{n+1} = 1 - \frac{\sigma_y\left(\bar{\varepsilon}_{n+1}^p\right)}{q_{n+1}}\left(C_\eta.B_{n+1}.\eta_{n+1} + A_{n+1}.D_{n+1}.\xi_{n+1}\right)$$

$$\beta_{n+1} = \frac{\sigma_y\left(\bar{\varepsilon}_{n+1}^p\right)}{q_{n+1}}\left[C_\eta.B_{n+1} - \frac{9.A_{n+1}.D_{n+1}}{2{q_{n+1}}^2}\left(tr({\boldsymbol{\sigma}_{n+1}}^2) - \frac{tr(\boldsymbol{\sigma}_{n+1})^2}{3}\right)\right]$$

$$\lambda_{n+1} = \frac{3.\sigma_y\left(\bar{\varepsilon}_{n+1}^p\right).A_{n+1}.D_{n+1}}{{q_{n+1}}^2} \quad ; \quad D_{n+1} = (C_\theta^{ax} - C_\theta^s)(1 - {\mu_{n+1}}^m)\frac{\cos(\pi/6)}{1-\cos(\pi/6)}\frac{\tan(\theta_{n+1} - \pi/6)}{\cos(\theta_{n+1} - \pi/6)}\frac{1}{\sin 3\theta_{n+1}}$$

(iv) Update the others state variables:

$$\boldsymbol{\varepsilon}_{d\;n+1}^e = \frac{1}{2G}\boldsymbol{S}_{n+1} \quad ; \; \varepsilon_{v\;n+1}^e = \frac{1}{K}p_{n+1} \quad ; \quad \boldsymbol{\varepsilon}_{n+1}^e = \boldsymbol{\varepsilon}_{d\;n+1}^e + \frac{1}{3}\varepsilon_{v\;n+1}^e\boldsymbol{I} \quad ; \; \bar{\varepsilon}_{n+1}^p = \bar{\varepsilon}_n^p + \Delta\bar{\varepsilon}^p$$

(v) Exit

3. CALIBRATION PROCEDURE

The Bai & Wierzbicki elasto-plastic model requires six material parameters $\left(C_\eta, \eta_0, C_\theta^s, C_\theta^t, C_\theta^c, m\right)$ and the material strain hardening function $\sigma_y(\bar{\varepsilon}^p)$ to be determined. According to Bai (2008), four experimental tests are performance, in order to determine the required parameters. The first one, a smooth bar specimen is selected in tensile loading condition and C_η, η_0 and $\sigma_y(\bar{\varepsilon}^p)$ are determined. After that, a notched bar specimen is carried out in order to determine the parameter C_θ^t. The set of parameters C_θ^c, C_θ^s and m are determined by a cylindrical specimen in the upsetting test and by a flat grooved plate tensile test. More details about the calibration of the materials parameters can be verified in Bai

(2008). In this paper, the materials parameters used were previously determined by Bai (2008) for an aluminum alloy 2024-T351. The parameters can be observed by the Table 1 below.

Table 1. Material parameters for aluminum alloy 2024-T351 (Bai, 2008)

Parameter		Value
Young's modulus	$E\ [MPa]$	71500
Poisson´s ratio	ν	0.33
Yield stress	$\sigma_{yo}\ [MPa]$	370
Stress strain curve	$\sigma_y(\bar{\varepsilon}^p)[MPa]$	$908.(0.0058+\bar{\varepsilon}^p)^{0.1742}$
Hydrostatic stress influence	C_η	0.09
Triaxiality ratio reference	η_0	0.33
Lode dependence - shear	C_θ^s	0.855
Lode dependence - tensile	C_θ^t	1.0
Lode dependence - compression	C_θ^c	0.9
Lode dependence - exponent	m	6.0

4. GEOMETRY AND MESH DEFINITION

In the following, the geometries of each specimen, which will be used in the numerical simulations, are presented as well as the meshes definition. Figure 1 shows the dimensions for both cylindrical smooth and notched bars with a notch radius equal to $R = 4\ mm$ and for a flat grooved plate specimen.

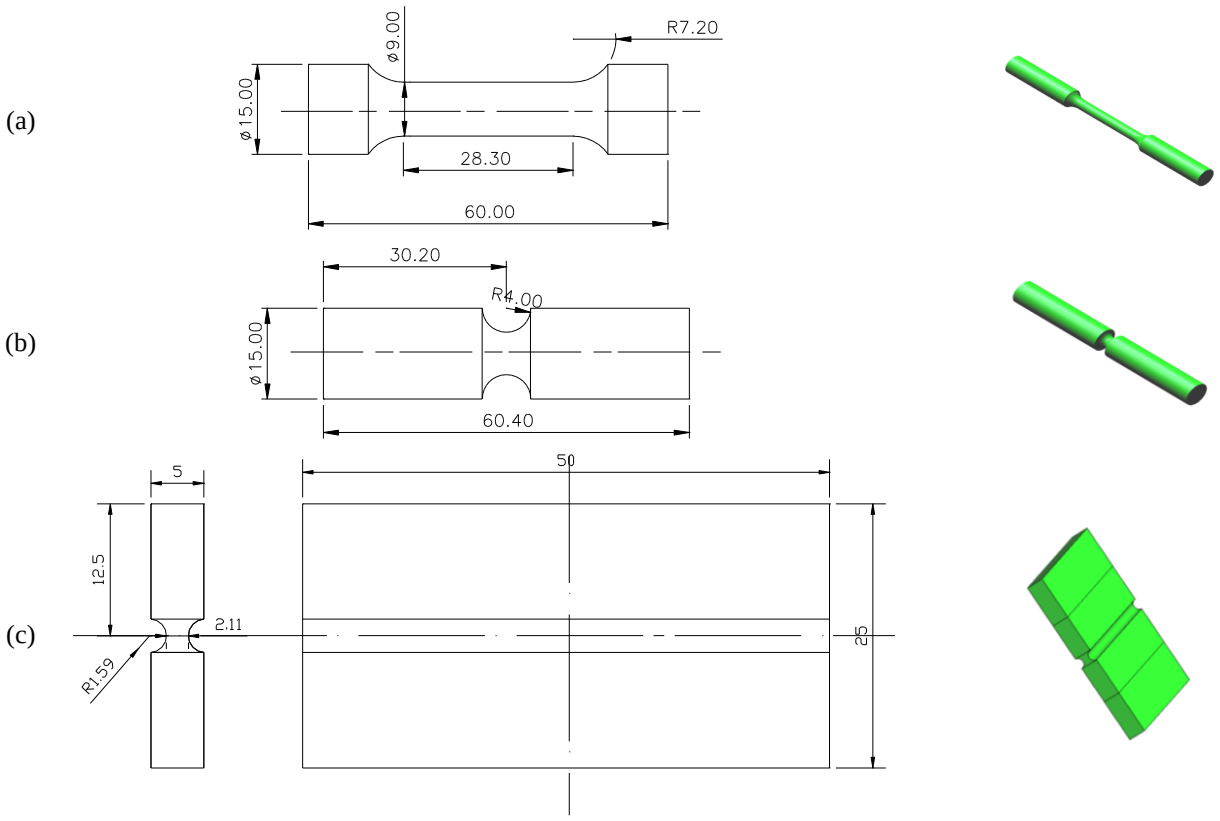

Figure 1. Geometry of the cylindrical smooth and notched bars, and for a flat grooved plate specimens (dimensions in mm), see Bai (2008).

In order to capture the necking pattern and the evolution of internal variables, a relatively fine discretisation is used in the region surrounding the smaller cross-section of the specimens (see Figure 2 and Figure 3). The standard eight-noded axisymmetric quadrilateral element, with four Gauss integration points, is adopted for both cylindrical bars. A total number of 1800 elements has been used in the discretisation of both the smooth bar (see Figure 1a) and the notched bar with radius of $R = 4\ mm$ (see Figure 1b), amounting to a total of 5581 nodes. In all cases, the gauge used is equal to $25.4\ mm$.

The stretching of a flat grooved plate is also used. The initial geometry of the specimen is shown in Figure 3. Due to symmetry, only one half of the geometry is simulated, with appropriate boundary conditions imposed to the symmetry plane. A three dimensional mesh of eight node elements, with four Gauss integration points, is used to discretise half of the specimen. A total number of 3000 elements have been used amounting to a total of 4743 nodes. The gauge used is equal to 25.0 mm.

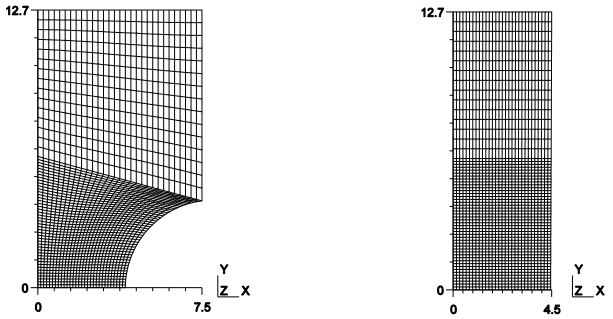

(a) (b)

Figure 2. Finite element meshes for the cylindrical notched bar (a) R = 4 mm and for the (b) smooth bar specimens.

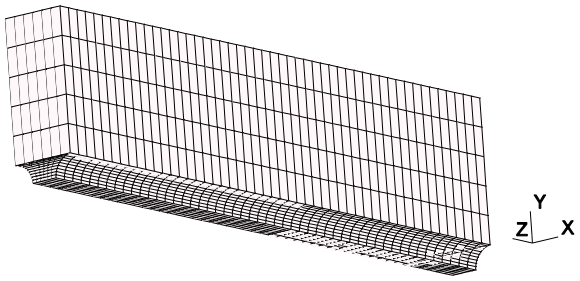

(a)

Figure 3. Finite element meshes for the flat grooved plate specimen with R = 1.59 mm.

5. NUMERICAL RESULTS

According to the numerical simulations, three types of specimens were used, regarding different levels of triaxiality ratio and Lode angle. The Bai & Wierzbicki model were set up, regarding three different cases: case 1 represents the Bai & Wierzbicki model without both pressure effect and Lode angle dependence, case 2 represents the model only with pressure effect active and case 3 represents the model with both pressure effect and Lode angle dependence.

Figure 4 represents some numerical results for reaction versus displacement curve and for the evolution of the equivalent plastic strain at the critical point. For the smooth bar specimen (Figure 4a), which is used as calibration reference point, both curves are very similar and the contribution of the hydrostatic stress and Lode angle over the plastic flow rule can be negligible. Nevertheless, for the notched bar specimen (Figure 4b), the numerical results with both pressure and Lode angle active are more realistic than without both effect. In this case, the difference between the reaction versus displacement curve without both effects and the experimental curve is around 6%. Regarding the activation of both effects, in the same case, the difference reduces to less than 1%, which can highlight the importance of pressure and Lode angle in the behavior of ductile materials. For the flat grooved plate specimen (Figure 4c), the correction on the reaction versus displacement curve, regarding both effects is more visible and, in this case, the difference between the model without effects and the experimental curve is around 20%, which is reduced to less than 2%, when both pressure effect and Lode angle dependence are active. The contribution of both effects can also be observed, regarding the evolution of the equivalent plastic strain, which for the flat grooved plate specimen presents different rates. Table 2 represents the difference between numerical and experimental results for the reaction versus displacement curves, regarding the activation of each effect for the specimens used.

Table 2. Difference between numerical and experimental results for the reaction versus displacement curve.

Specimen	Case 1 – without effects	Case 2 – with only pressure effect	Case 3 – with both pressure effect and Lode angle dependence
Smooth bar	1%	1%	1%
Notched bar R = 4.0 mm	6%	4%	1%
Flat grooved R = 1.59 mm	20%	16%	1%

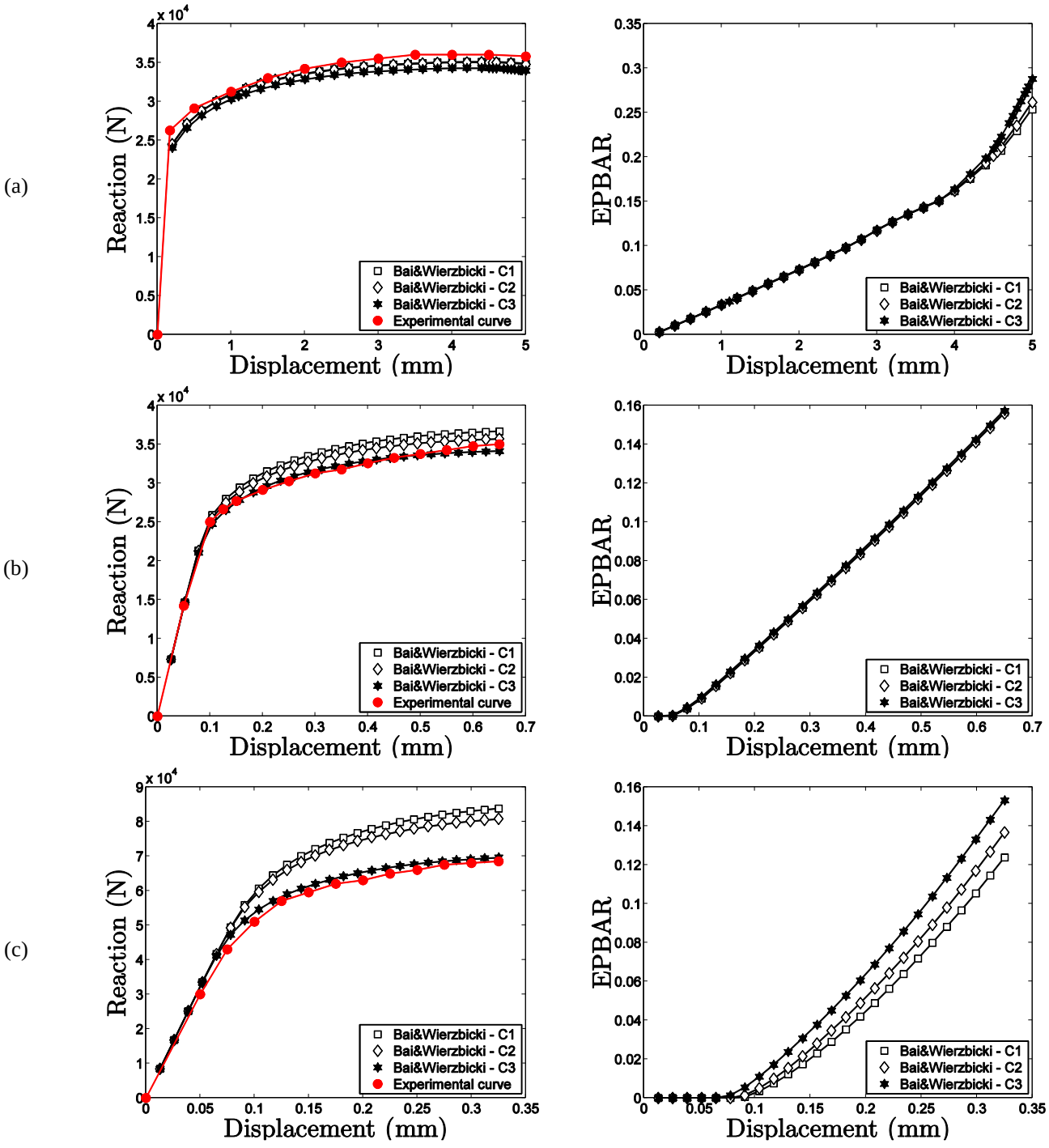

Figure 4. Reaction versus displacement curves and evolution of the equivalent plastic strain, regarding (a) a smooth bar specimen, (b) a notched bar specimen with R = 4.0 mm, and (c) a flat grooved plate specimen with R = 1.59 mm.

The contour of the equivalent plastic strain can also be analyzed, in order to verify the ability to predict crack initiation. Some authors, as Freudenthal (1950), Gillemont (1976) and Datcko (1966), have suggested the use of the plastic strain as a fracture indicator, thought the total plastic work or the equivalent plastic strain. Nevertheless, researchers as Wilson (2002) and Gouveia (1995) have shown that this parameter is not enough to be used as fracture indicator, and in some cases, can indicate potential sites to fracture beginning in disagreement with experimental evidences. According Wilson (2002), for both smooth and notched bars specimens, the crack begins on the central node and grows to the surface of the specimens. Analyzing Figure 5 and regarding the equivalent plastic strain as fracture indicator, only the numerical results for the smooth bar specimen agree with experimental evidence. For the notched bar specimen, this internal variable is maximum in the surface (Figure 5b), which cannot be regarded as fracture onset. Then, we can also observe, that for both cylindrical specimens, the activation of pressure effect and Lode angle

dependence does not influence on the location of the maximum value of the equivalent plastic strain. However, according to experimental tests promoted by Bai (2008) for the flat grooved plate specimen, the crack starts on center of the specimen and propagates to the surface, in what can only be evidenced through the numerical results presented regarding both effects active (see Figure 5c)

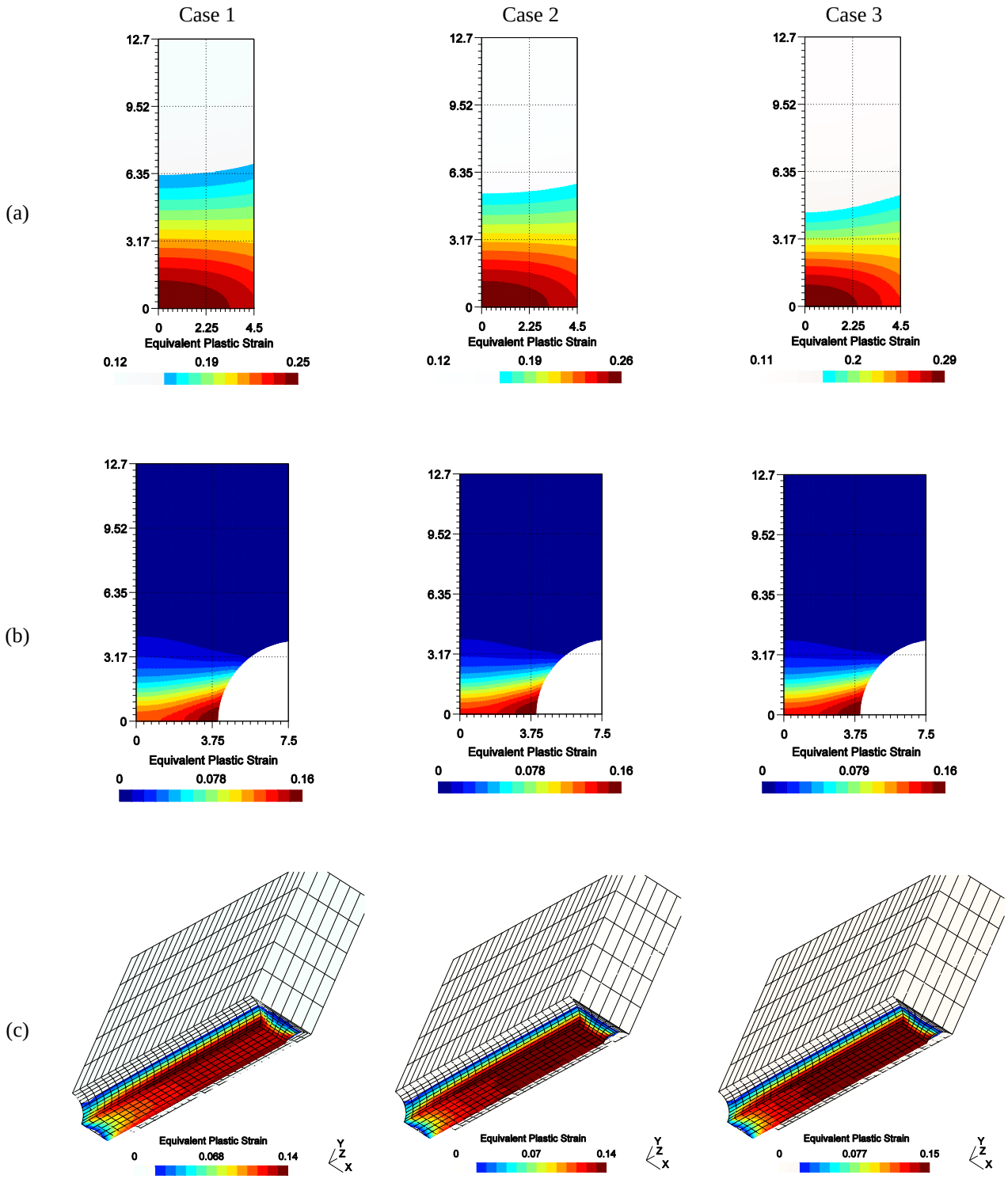

Figure 5. Contour of the equivalent plastic strain, regarding (a) a smooth bar specimen, (b) a notched bar specimen with R = 4.0 mm, and (c) a flat grooved plate specimen with R = 1.59 mm.

5. CONCLUSIONS

In this paper, the influence of both pressure effect and Lode angle dependence was studied thought a constitutive model proposed by Bai *et al* (2007) and an implicit numerical integration algorithm suggested by Malcher *et al* (2009). Specimens with different levels of triaxiality ratio and Lode angle were used as well as a material strongly dependent on both effects as an aluminum alloy 2024-T351. According to the numerical results presented, we can verify the importance of the hydrostatic stress and Lode angle on the plastic flow rule for ductile materials. The correction in the reaction versus displacement curves, when the effects are active, is evidenced mainly by numerical results for the flat grooved plate specimen. In this critical case, the curve without both effects presents an error of 20%, regarding the experimental data. Introducing both parameters, the agreement between numerical and experimental data was very satisfactory.

6. ACKNOWLEDGEMENTS

The authors acknowledge the support of Portuguese Science and Technology Foundation (FCT) and the support of University of Brasília, Faculty UnB at Gama (FGA).

7. REFERENCES

Bai, Y., 2008, Effect of Loading History on Necking and Fracture. Ph.D Thesis, Massachusetts Institute of Technology.

Bai, Y., Wierzbicki, T., 2007, A new model of metal plasticity and fracture with pressure and lode dependence, International Journal of Plasticity, doi:10.1016/j.ijplas.2007.09.004.

Bardet, J. P., 1990, Lode Dependence for Isotropic Pressure-Sensitive Elastoplastic materials. Journal of Applied Mechanics, 57:498-506.

Brünig, M., Berger, S., Obrecht, H., 2000, Numerical simulation of the localization behavior of hydrostatic-stress-sensitive metals. International Journal of Mechanical Sciences, 42:2147-2166.

Brünig, M., 1999, Numerical simulation of the large elastic-plastic deformation behavior of hydrostatic stress-sensitive solids: International Journal of Plasticity.

Datsko, J., 1966, Material Properties and Manufacturing Process. New York: John Wiley & Sons.

De Souza Neto, E.A., Peri´c, Owen, D.R.J., 2008, Computational methods for plasticity: theory and applications. John Wiley & Sons Ltd.

Freudenthal, A., 1950, The Inelastic Behavior of Engineering Materials and Strucutures. New York: John Wiley & Sons.

Gillemont, L., 1976, Criterion of crack initiation and spreading. Engineering Fracture Mechanics , pp. 239-253.

Gouveia, B., Rodrigues, J., & Martins, P., 1995, Fracture Predicting in Bulk Metal Forming. International Journal of Mechanical Sciences , pp. 361-372.

Karr, D. G., Law F. P., Fatt M. H., and Cox G. F. N. 1989, Asymptotic and quadratic failure criteria for anisotropic materials. International Journal of Plasticity, 5(4):303-336

Malcher, L. ; Andrade Pires, F.M. ; César de Sá, J.M.A ; Andrade, F.X.C., 2009, Numerical integration algorithm of a new model for metal plasticity and fracture including pressure and Lode angle dependence. International Journal of Material Forming - Springer, 2:443-446.

Richmond, O., & Spitzig, W.A., 1980, Pressure dependence and dilatancy of plastic flow. In Theoretical and Applied Mechanics, Proceedings of the 15th International Congress of Theoretical and Applied Mechanics., pages 377–386, Toronto, Ont, Can, North-Holland Publ Co, Amsterdam, Neth.

Simo, J., & Hughes, T., 1998, Computational Inelasticity. Springer.

Wilson, C.D., 2002, A critical reexamination of classical metal plasticity. Journal of Applied Mechanics, Transactions ASME, 69(1):63–68, ISSN 0021-8936.